Bioinspired extremotolerant glycerogels

Md. Tariful Islam Mredha
Chonnam National University
Yoonseong Lee
Chonnam National University
Adith Varma Rama Varma
Chonnam National University
Tanish Gupta
Chonnam National University
Rumesh Rangana Manimel Wadu
Chonnam National University
Insu Jeon (i_jeon@chonnam.ac.kr)
Chonnam National University

Article

Keywords:

Posted Date: March 22nd, 2022

DOI: https://doi.org/10.21203/rs.3.rs-1473122/v1

Abstract

Inspired by the “tun formation” of tardigrades, the hardest species on the planet, a new class of extremotolerant glycerogels with well-modulated polymer structure, functions, and properties was developed. Glycerogels comprising extremoprotected intra- and inter-molecular networks were fabricated by smooth replacement of water in predesigned hydrogels with glycerol, followed by thermal annealing. Four different glycerogels were fabricated as proofs-of-concept using different crosslinkers and polymers; they exhibited a wide range of stiffness, strength, stretchability, and toughness, as well as elasticity, plasticity, hysteresis, self-recoverability, thermal-shock-absorption capability (150°C), and prolonged stability over an extremely wide temperature range (-50–80°C). The self-weldability of glycerogels, stretchable electrical patterns on glycerogels, and glycerogel-based electrolytes and supercapacitors demonstrate the complex 3D designability and facile functionalization capability of glycerogels. The variety of functional glycerogels developed herein offers opportunities to design diverse extremotolerant, flexible, and stretchable devices for bio, electrical/electronic, and soft robotic applications.

Introduction

Gels, a class of semisolid materials formed by crosslinked 3D polymer networks swollen in specific solvents, have attracted significant attention owing to their applications in biomedicine, flexible electronics, energy-storage device, sensor/actuator, and soft robotics; they exhibit a wide variety of functions that no other solid or liquid material can exhibit solitarily[1–7]. Owing to their highly solvated polymer networks, gels inherently exhibit tissue-like structures, biocompatibility, cell-friendliness, and numerous biological functionalities[1–4]. They can be tailored to achieve specific electrical, thermal, actuation, shape-morphing, and stimuli-responsive properties owing to their simultaneous solid- and liquid-like nature[5–10].

Hydrogels are formed by water-swollen hydrophilic polymer networks and are widely used owing to their biocompatibility and immense scope for biomedical applications[1–4, 11,12]. To overcome the mechanical weakness of conventional hydrogels, several mechanically robust hydrogels—double-network[2,13], ionic/covalent[14], nanocomposite[15], polyampholyte[16], dynamically crosslinked[9,17], and hydrophobic/hydrophilic[18]—have been developed. However, their short lifetime in air limits their applications[1,10,19,20], particularly under harsh environmental conditions. Recently, several methods have been developed to improve the air-stability of hydrogels. For example, double-hydrophobic-coated hydrogels have long-term air-stability[19]. Various glycol/water-based organohydrogels that possess good antifreezing capabilities at subzero temperatures have been reported[20–24]. Photoresponsive gels based on metal coordination bonding have been developed from glycerol/water mixtures; such gels are functional at subzero temperatures[21]. A gel fabricated from ethylene glycol/water mixture had good negative-temperature ionic conductivity[22]. However, none of the aforementioned gel materials can be used at both temperature extremes (cold and hot). Therefore, it is challenging to establish a broad

concept of developing gel materials whereby various crosslinking/toughening mechanisms and gel functionalities would be durable under both extremely low and high temperatures.

Tardigrades are the most resilient lifeform on earth and can survive under extreme conditions—extremely low and high temperatures and pressures, dry weather, and intense irradiation[25–29] (Fig. 1a). Under harsh environmental conditions, tardigrades undergo a structural transition into a form known as the “tun state” by slowly squeezing out most of their nonbonded free water and simultaneously producing cell-protecting molecules such as sugars (including trehalose and glycerol) and proteins[27–29]. These molecules construct intra- and inter-molecular bonding networks between themselves and with biomolecules and cells to prevent irreversible damage under exposure to harsh conditions.

Inspired by the tun formation of tardigrades, a novel class of gel materials was designed using glycerol, which is a low-molecular-weight polyol that can retain its polymeric structure, functions, and properties under extreme conditions. Furthermore, glycerol is a bioderived green solvent that is rich in hydroxyl groups and forms a facile H-bonding network within itself and with various hydrophilic polymers[30,31] (Fig. 1b). Glycerol exhibits excellent supercooling up to its glass transition temperature (-83°C), extremely low vapor pressure (1 mmHg at 125°C), and extremely high boiling temperature (290°C)[31,32]. Pure glycerol was adopted as the extreme protectant molecule for the gel network because it functions similar to sugar and protein in protecting the tun state.

Our thorough review confirmed that most polyol solvents are unsuitable for fabricating gels with good structural integrity because their high viscosity and polymerization-induced phase separation decrease the degree of polymerization, hindering the 3D gel-structure formation (Supplementary Fig. 1). In contrast, numerous hydrogels are reported with a wide variety of functions[1–9,11–18]. In this study, various predesigned functional hydrogels were used as base materials. By harnessing the high water–glycerol affinity due to H-bond formation, the water in the gel network was replaced with glycerol without disrupting the polymeric structures and functions of the original hydrogels via a process that closely resembles tardigrades’ structural transition (Fig. 1c).

For most hydrogels, directly exchanging the original solvent with a viscous organic solvent leads to undesired phase separation and polymer aggregation because the high osmotic pressure of viscous solvents or alterations in polymer–solvent affinities drastically deswells the gel[33]. Further, upon immersing a typical water-equilibrated poly(vinyl alcohol) (PVA) hydrogel in glycerol, the gel squeezes out most of its water and shrinks to a weight fraction (W) of 38% (Fig. 1c). Therefore, direct solvent exchange results in hard, brittle, plastic-type gels (Supplementary Fig. 2). A stepwise slow exchange of the original solvent can prevent structural collapse of water-stable hydrogels (Fig. 1c), thereby preventing or significantly reducing gel shrinkage. In the case of water-swelling hydrogels (such as polyacrylamide (PAAm) hydrogels), rapid solvent exchange (instead of slow exchange) at higher temperatures can prevent swelling-induced structural collapse. Upon completion of solvent exchange, undesired residual stresses on the gel network can be released by thermal annealing of the gel. Herein, we propose a simple two-step process that enables the fabrication of a wide range of extremotolerant glycerogels (GGs) from

predesigned hydrogels without sacrificing the structural and functional properties of the original hydrogels.

Results

Extremotolerant GGs

Four basic GGs were fabricated using different polymers and crosslinking strategies: PAAm GGs (using a covalent crosslinker); PVA GGs (by H-bonding); poly(acrylamide-co-acrylic acid)/Iron(III) (P(AAm-*co*-AAc)/Fe^{3+}) GGs (using dual crosslinkers (covalent and Fe^{3+}-coordination)); and cellulose GGs (by H-bonded pure biopolymer structure) (Fig. 2). The GGs exhibited excellent long-term stability (~ 7 d) over −50–80°C. Upon exposure to air at -50, 25, and 80°C for 1 week, the weight change of all the gels remained within ± 10 wt.% (Fig. 3a and b, and Supplementary Fig. 3). The small increase or decrease in weight was caused by the absorption of atmospheric moisture or the loss of glycerol from the gel network, respectively.

The natures and structures of the different polymers and crosslinkers facilitated the systematic fabrication of a variety of GGs with wide-range tunable mechanical performance (Fig. 3c–f, Supplementary Figs. 4–7). For example, loosely crosslinked soft PAAm GG stretched > 1200% and exhibited low modulus (0.09 ± 0.003 MPa) and strength (0.22 ± 0.02 MPa). The strong H-bonding, semicrystalline nature, and excellent energy-dissipation capability of PVA resulted in PVA GG with high stiffness (8.9 ± 0.2 MPa) and strength (8.5 ± 0.01 MPa) and extremely high work of extension (49.9 ± 0.4 MJ m^{-3}). Dual-crosslinked P(AAm-*co*-AAc)/Fe^{3+} GG exhibited a good balance of stiffness (1.6 ± 0.1 MPa), strength (7.1 ± 0.3 MPa), and work of extension (23.5 ± 4.6 MJ m^{-3}) owing to the good energy-dissipation capability because of its strong ion-coordinated structure. Physically crosslinked cellulose GG exhibited high stiffness (9.4 ± 0.9 MPa) and strength (2.9 ± 0.1 MPa) and low stretchability (~ 100%) owing to the highly solvated elongated structure of rigid linear polymers, which have large persistence lengths[11]. By varying the monomer, polymer, and crosslinker compositions, the mechanical properties of each GG developed herein could be tuned further. Most importantly, the mechanical properties of all the GGs remained nearly unchanged following exposure to air for 7 d at extremely low (-50°C), room (25°C), and extremely high (80°C) temperatures (Fig. 3c–f, Supplementary Fig. 4–7). The extremotolerance of the gels was demonstrated by extending and relaxing them at -50 and 80°C (Fig. 3g and h, and Supplementary Movie 1–4) and applying a thermal shock of 150°C for 10 min to the GG and hydrogel (Supplementary Figs. 8 and 9). The GG survived without any significant changes in weight and stretchability, but the corresponding hydrogel dried out completely. The roadmap for designing extremotolerant GGs is shown in Fig. 2; it should be applicable for various functional polymers and crosslinkers suitable for hydrogel fabrication.

Fracture toughness

The toughness of the as-fabricated GGs was evaluated by fracture tests using notched and unnotched samples (Fig. 4a and b). Fracture energies vary significantly with the polymer and crosslinker types. All the developed GGs exhibited excellent fracture toughness; PAAm and PVA GGs exhibited the minimum (1581 J m^{-2}) and maximum (19,627 J m^{-2}) fracture energies, respectively (Fig. 4c). The GGs had significantly higher fracture toughness than their corresponding hydrogels (Supplementary Fig. 10). The increased inter- and intra-molecular H-bonding network caused by the three hydroxyl arms of glycerol than that by the single hydroxyl arm of water is inferred as the principal contributor to the higher fracture resistance of the GGs than that of their hydrogel counterparts. Thereafter, the dynamic noncovalent bonds (H-bonds, ion-coordination) with an appropriate balance of weak and strong crosslinking points in the P(AAm-*co*-AAc)/Fe^{3+} and PVA GGs granted them extreme toughness exceeding that of natural rubbers, most biological tissues, and tough soft materials reported to date[1,7,14,16–18].

Hysteresis, elasticity, plasticity, and self-recoverability

The elasticity, plasticity, energy dissipation, and self-recoverability of GGs can be modified using various crosslinkers and polymers. The covalently crosslinked soft PAAm GG exhibited high nonlinear elasticity with a marginal hysteresis despite ~ 500% loading–unloading (Fig. 4d), similar to PAAm hydrogel behavior[34]. The hysteresis and strength of the PAAm GG recovered within 5 min of load-unload testing. These results suggest that the PAAm chain in the GG system has similar dynamics and structure as the hydrogel system. Unlike the PAAm GG, the PVA GG exhibited significant hysteresis with a large plastic strain (~ 250%) at 500% loading–unloading (Fig. 4e). The hysteresis was ~ 94% of the total work done during the 500% stretch, proving the excellent energy-dissipation capability derived from sacrificial bonds (H-bonds). The hysteresis and majority of the strain remained unrecovered 12 h after the load-unload testing, indicating the plastic deformation of PVA GG, which is atypical of general hydrogels. The softer PVA GGs (tensile strength < 1 MPa), which were prepared with extremely low polymer concentrations (5 and 3 wt.%), exhibited similar plastic behavior (Supplementary Fig. 11). PVA GG had marginal hysteresis in the low strain region (Supplementary Fig. 12), evidencing its good self-recoverability. Following 50 loading–unloading cycles at 10% tension, the hysteresis and strength (~ 0.65 MPa) of the gel recovered completely within 20 min.

The dual-crosslinked P(AAm-*co*-AAc)/Fe^{3+} GG also exhibited significant hysteresis at 150% strain, indicating energy dissipation via sacrificial bonds (ion-coordination) (Fig. 4f). Unlike PVA GG, most hysteresis and strength of P(AAm-*co*-AAc)/Fe^{3+} GG were recovered within 30 min, suggesting the near-reversibility of sacrificial bonds. The gel exhibited good recoverability with marginal hysteresis up to 50% strain, and the recovery time for strength and hysteresis decreased to 5 min (Supplementary Fig. 13a). The excellent self-recoverability of the gel was further demonstrated by loading the sample at ~ 50% tension followed by unloading it for 50 cycles (Supplementary Fig. 13b). Most strength and hysteresis of the gel were recovered within 20 min. The cellulose GG exhibited lower stretchability than the other GGs (< 150%) because of its large glycerol content and rigid nature of the cellulose polymer[11]. However, cellulose GG exhibited significant hysteresis at 20% strain, suggesting efficient energy dissipation by the

H-bonds in the cellulose network (Fig. 4g). Most hysteresis and strength recovered within 30 min, indicating the reversibility of sacrificial bonds. These results strongly suggest that a wide variety of GGs with tunable elasticity, plasticity, hysteresis, self-recoverability, and fatigue resistance can be designed by controlling the polymeric and crosslinked structure.

The excellent plasticity of PVA GG was studied in depth by applying repetitive strain of increasing magnitude (Fig. 4h). During the cycles, the gel exhibited plastic behavior with accumulated strains. The softer PVA GGs exhibited similar behavior (Supplementary Fig. 14). The ratio between the accumulated and applied strains increased significantly with the magnitude of the applied strain (Supplementary Fig. 15). High-polymer-density PVA GGs exhibited high accumulated–applied strain ratios. These results suggest that PVA GG can be modulated with tunable plastic behavior. These properties are difficult to achieve with common viscoelastic soft materials. Thus, soft devices with complex 3D configurations or patterned structures can be fabricated by plastically deformed bending/twisting/rolling/patterning.

Self-welding

The versatile applicability of the GGs was further extended by their excellent self-welding capabilities. A self-welding method was developed for efficiently joining cellulose-based hydrogels via ion-induced polymer reconfiguration[12], which was applied to GG systems. The welding efficiency was quantitatively determined by conducting the lap shear test on coaxially joined GGs (Fig. 5a, b). The welded cellulose GG exhibited an adhesive strength of 0.77 MPa, significantly higher than adhesive hydrogels[35] and similar to cartilage–bone[36] or hydrogel–bone bonding[2,37]. Furthermore, the welded sample stretched > 100%, demonstrating the excellent bonding toughness. Similar to the cellulose GG, the welded soft PVA GG (fabricated from a 5 wt.% PVA precursor) exhibited good adhesive strength (0.21 MPa) (Supplementary Fig. 16).

Fractal-patterned GGs for stretchable electrical/electronic devices

Various tailor-made functionalized GGs have demonstrated their potential for diverse next-generation electrical/electronic applications. Electrically conductive GGs have been prepared by coating silver onto GGs via high-speed ion sputtering[38]. Using a predesigned mask (Supplementary Fig. 17), a thin layer of a simple fractal-designed[39] silver pattern loop has been created flawlessly on a soft PVA GG (Fig. 5c). Facile LED lighting using the patterned GG suggested that the silver pattern was sufficiently well-connected at a microscopic level and completed the circuit (Fig. 5d, Supplementary Movie 5). The stability and stretchability of the patterned GG were demonstrated at -50, 25, and 80°C (Fig. 5e–g, Supplementary Movies 6–8), at which the gel stretched and recovered almost completely undamaged, demonstrating the formation of a highly stable pattern with resilient polymer–metal interactions on the gel surface.

GG electrolytes for energy-storage devices

Ionically conductive GGs have been developed. Because of their hydrophilicity and polarity, glycerols readily dissolve numerous common inorganic salts. For instance, $LiClO_4$ is widely used in preparing battery and supercapacitor electrolytes[40,41] and is soluble in glycerols at large concentrations. Therefore, as an example, $LiClO_4$-ion-loaded PVA GG electrolytes were prepared by simple diffusion-induced ion loading[42]. Thereafter, a prototype supercapacitor was fabricated by sandwiching an as-prepared PVA GG electrolyte sheet (~ 0.2 mm thick) between two carbon nanotube (CNT)-based flexible electrode films. The subsequent annealing step induced strong electrode–gel-surface self-attachment, imparting excellent mechanical stability to the device. Consequently, the device exhibited high flexibility under bending and twisting with no interfacial failures (Fig. 6a, Supplementary Movie 9). The PVA GG electrolyte exhibited an ionic conductivity of 0.021 ± 0.006 S m^{-1} at 25°C. The conductivity decreased and increased with decrease and increase in the temperature, respectively (Fig. 6b), which was attributed to the change in solvent viscosity with temperature. The GG attained an extremely high conductivity of 0.11 ± 0.03 S m^{-1} at 80°C and maintained a good conductivity of 0.003 ± 0.0003 S m^{-1} at -20°C, similar to that of gel electrolytes used for energy-storage devices[22,42–44].

The supercapacitor exhibited a quasi-rectangular closed loop on the cyclic voltammogram (CV), suggesting a perfect electric double-layer capacitor (EDLC) behavior. Even at higher scan rates, the device exhibited similar CV patterns within the 0–1 V voltage window (Supplementary Fig. 18). The galvanostatic charge/discharge (GCD) curves also exhibited a symmetric triangular shape at different current rates, confirming perfect EDLC behavior (Supplementary Fig. 19). The areal capacitance was calculated as 5.29 ± 0.24 mF cm^{-2} at 1 mV s^{-1} (CV curve) and 7.46 ± 0.63 mF cm^{-2} at 0.1 mA (GCD curve). The areal capacitance obtained from the CV and GCD curves remained nearly unchanged with scan rate and current density variations. Furthermore, the device exhibited excellent performance from −20 to 80°C (Fig. 6c, d). The CV curves followed closed quasi-rectangular loops. The areal capacitance of the device was 5.97 ± 0.49 and 2.21 ± 0.36 mF cm^{-2} at 80 and − 20°C, respectively. The change in areal capacitance with temperature closely resembles the change in ionic conductivity of the GG electrolyte at the respective temperatures.

Discussion

Herein, a novel class of extremotolerant GGs with wide-range tailor-made properties and functionality was developed using a simple two-step tardigrade-inspired technique. Initially, the water-to-glycerol solvent exchange of the predesigned hydrogels was conducted slowly (stepwise) for the water-stable equilibrated hydrogels (PVA, cellulose, and P(AAm-*co*-AAc)/Fe^{3+}) and rapidly (at high temperatures) for the water-swellable as-prepared hydrogel (PAAm). Thereafter, the as-prepared gels were thermally annealed to relieve undesired residual stresses on the gel network and uniformly distribute the polymers and crosslinking structures. The wide-temperature-tolerant glycerol builds an extremoprotected network via intra- and inter-molecularly H-bonds with various hydrophilic polymers, and creates a suitable microenvironment for various crosslinking structures and toughening mechanisms, paving the way for diverse functionalization. Lacking an energy-dissipation mechanism, a soft polymer (PAAm) with loose

covalently crosslinked structures imparted extremely high stretchability and rapid self-recovery. Extremely high toughness, stretchability, and strength of PVA GGs are achieved because of the efficient energy dissipation facilitated by high-density sacrificial H-bonds in soft PVA polymers. In PVA GGs, the plastic deformation caused a large irreversible hysteresis. The efficient and reversible energy dissipation of dual-crosslinked (covalent and ion-coordination) GGs produced a balance of softness, strength, and toughness with low hysteresis and excellent self-recoverability. H-bond-based GGs fabricated from rigid natural polymers (such as cellulose) had lower stretchability than soft PVA GGs but showed excellent stiffness, strength, and toughness owing to their efficient energy dissipation. Rigid natural polymers can be used to fabricate GGs with various biomimetic superstructures. Irrespective of the polymeric and crosslinked structures, the GGs demonstrated excellent stability from − 50 to 80°C. Long-term stability over such a wide temperature range has not been achieved for soft materials to date. High thermal-shock-absorption ability at 150°C further confirms the durability of extremoprotected network under harsh conditions.

Physically crosslinked GGs exhibited excellent self-welding capabilities imparted by ion-induced structural reconfiguration, which confers a significant advantage in designing various extremotolerant devices with complex 3D structures. GGs with various extraordinary functions can be developed by rationally integrating various functional materials. A stretchable electroconductive GG was fabricated by ion-sputtering a fractal-shaped silver pattern on the GG surface. In general, metal deposition on soft materials is difficult because high-speed ion-sputtering generates much heat around the sputtering region. The structural and thermal stability of GGs and atomic-scale polymer–silver-particle adhesion facilitated the stretchability of the hybrid GG from − 50 to 80°C without any interfacial failure. Thereafter, the performance of GG-based electrolyte and a prototype flexible supercapacitor were also studied. Excellent ion solvation and extremoresistance of glycerol induced good ion-conduction pathways in the GG-based electrolyte. Therefore, the fabricated supercapacitor exhibited excellent capacitance (2.2–6 mF cm^{-2}) from − 20 to 80°C, behaving similar to several recently reported high-performance supercapacitors (Supplementary Fig. 20)[22,45–49]. Stretchable, electrically conductive, and ionically conductive GGs can enhance the applicability of soft materials to next-generation extremotolerant energy-storage devices, sensors or actuators, and soft robotics. This study will facilitate the rational design of a wide range of extremotolerant GGs that can satisfy stringent next-generation requirements by harnessing currently available hydrogels that have wide-range functionality and properties.

Methods

Materials. Acrylamide (AAm), acrylic acid (AAc), *N,N'*-methylenebisacrylamide (MBAA), dimethyl sulfoxide (DMSO), propylene glycol, and iron(III) chloride ($FeCl_3$) were purchased from Daejung Chemicals & Metals Co., Ltd. (Republic of Korea). Glycerol, ethylene glycol, *N,N'*-dimethylacetamide (DMAc), ethanol, and lithium chloride (LiCl) were purchased from Samchun Pure Chemical Co. Ltd. (Republic of Korea). Cellulose-based filter paper (ADVANTEC) was purchased from Toyo Roshi Kaisha Ltd. (Japan). Poly(vinyl alcohol) (PVA; M_w: 89,000–98,000), ammonium persulfate (APS), and lithium perchlorate ($LiClO_4$) were

purchased from Sigma Aldrich. Tripropylene glycol (TriPG) was purchased from Acros Organics (Belgium). Carbon nanotube film (CNT) (thickness: 10–20 mm) was purchased from Chengdu Organic Chemicals Co., Ltd., Chinese Academy of Sciences (China). All chemicals were used directly without further purification. Ultrapure deionized water was used in the experiments as required.

Fabrication of polyacrylamide glycerogels (PAAm GGs). Initially, the PAAm hydrogel was prepared via free-radical polymerization as follows: A precursor solution containing 3 M of AAm monomer, 0.05 mol% (with respect to monomer concentration) of MBAA crosslinker, and 0.1 mol% (with respect to monomer concentration) of APS initiator was prepared using deionized water. The solution was poured into a rectangular mold that was prepared by sandwiching a silicone rubber gasket of 3 mm thickness between two flat plastic plates. Thereafter, polymerization was conducted by incubating the mold at 60 °C for 8 h. The as-prepared PAAm hydrogel was removed from the mold and immersed in preincubated glycerol at 60 °C for 2 h to rapidly exchange the water with glycerol. Thereafter, the gel was immersed in glycerol for 3 d at 25 °C to ensure the complete exchange of water with glycerol. The as-prepared GG was dry-annealed in a closed glass vial at 100 °C for 3 h, followed by slow cooling to 25 °C to obtain the desired PAAm GG (thickness ≈ 2.6 mm), which was used for further characterization.

Fabrication of poly(vinyl alcohol) glycerogels (PVA GGs). Initially, PVA hydrogel was prepared by freeze-thawing, as described in a previous study[11], with slight modifications. A PVA solution was prepared by dissolving PVA powder in a DMSO/water (75:25, w/w) mixture under continuous stirring at 140 °C overnight. DMSO/water mixture is known to produce fine crystals of PVA chains at subzero temperatures[50]. Unless otherwise noted, a 10 wt.% PVA precursor solution was used to fabricate the original PVA GG. The solution was inserted into a rectangular plastic mold of 3 mm thickness (prepared by sandwiching a silicone rubber gasket between two plastic plates). Thereafter, the mold containing the polymer solution was incubated at -50 °C for 1 d, followed by thawing at 25 °C for 12 h. The gel formed was removed from the mold and immersed in water for 3 d. The water was replaced repeatedly to obtain a water-equilibrated PVA hydrogel. This gel was immersed sequentially in aqueous glycerol solutions of 25%, 50%, 75%, and 100% glycerol content for 12, 12, 24, and 24 h, respectively, to obtain PVA GG. The as-prepared GG was annealed in a closed glass vial at 120 °C for 6 h, whereafter it was slowly cooled to 25 °C to obtain the desired PVA GG (thickness ≈ 1.8 mm), which was used for further characterization.

Fabrication of poly(acrylamide-co-acrylic acid)/Iron(III) glycerogels (P(AAm-*co*-AAc)/Fe^{3+} GGs). Initially, a P(AAm-*co*-AAc) hydrogel was prepared by the free-radical copolymerization of AAm and AAc. A precursor solution containing 3 M AAm and 0.6 M AAc in the presence of 0.1 mol% MBAA and 0.1 mol% APS (with respect to total quantity of monomers) as crosslinker and initiator, respectively, was prepared in water. The solution was inserted into a plastic mold (prepared by sandwiching a silicone rubber gasket between

two plastic plates) of 2 mm thickness and polymerized at 60 °C for 8 h. The as-prepared (P(AAm-*co*-AAc) hydrogel was removed from the mold and immersed in a 0.075 M aqueous $FeCl_3$ bath for 1 d for ion binding. Thereafter, the superfluous ion from the gel was removed by washing it in pure water for 1 d to obtain the desired water-equilibrated (P(AAm-*co*-AAc)/Fe^{3+} hydrogel. Subsequently, the as-prepared GG was obtained by sequential solvent exchange process (0%→25%→50%→100%), similar to the process described for fabricating the PVA gel. The as-prepared GG was initially wet-annealed in a glycerol bath at 120 °C for 2 h and subsequently cooled slowly to 25 °C. The gel was then subjected to closed dry annealing at 120 °C for 6 h and slowly cooled to 25 °C to obtain the desired P(AAm-*co*-AAc)/Fe^{3+} GG (thickness ≈ 1.6 mm), which was used for further characterization.

Fabrication of cellulose glycerogels (cellulose GGs). Initially, cellulose hydrogels were prepared using cellulose paper. Small pieces of cellulose filter paper were sequentially washed using water (~6 h), ethanol (~6 h), and DMAc (~12 h), whereafter they were vacuum dried at 60 °C. A 1.5% (w/w) cellulose solution was prepared by dissolving the cellulose paper in a DMAc/LiCl (92:8, w/w) solvent. The cellulose solution was cast into a flat glass mold of 3 mm depth and exposed to ambient conditions (temperature: ~25 °C; humidity: 30–60%) for ~3 d to induce gelation of the cellulose through H-bond formation. The as-prepared organogel was sequentially equilibrated in ethanol (1 d) and water (1 d) to obtain a cellulose hydrogel. The water in the hydrogel network was replaced with glycerol through the sequential solvent exchange process (0%→25%→50%→100%) described earlier, and subsequently dry-annealed in a closed glass vial at 120 °C for 6 h and finally cooled slowly to 25 °C to obtain the cellulose GG (thickness ≈ 2 mm), which was used for further characterization.

Mechanical characterization. All the mechanical tests were performed under ambient conditions (humidity: 30–60%; temperature: ~25 °C) using a TEST ONE TO-100-1C universal testing machine (Republic of Korea) equipped with a 10 kgf load cell.

For tensile failure and loading–unloading tests, gel sheets (thickness: 1.6–2.6 mm) were cut into rectangular shapes (length: ~30 mm; width: ~3 mm). The samples were clamped along the longitudinal direction while maintaining a distance of ~10 mm between the clamps. Tests were performed by moving the upper clamp. Deformation was carried out at 500%/min (0.083 s^{-1}) for tensile tests and 100%/min (0.017 s^{-1}) for cyclic loading–unloading tests. To evaluate the effect of temperature on the mechanical properties, the samples were initially incubated in a chamber at the respective temperature for 7 d. Thereafter, the samples were extracted from the respective chambers and immediately mounted onto the tensile tester for testing. To evaluate the mechanical properties, three tests were performed for each type of gel under each condition. The data are presented as mean values with absolute deviations.

The fracture toughness of the GGs was evaluated using tensile fracture tests. Force–displacement curves were constructed from the data obtained from tensile tests conducted using notched and unnotched samples for each type of GG. The rectangular sample sheets were precut to a width (w) of 20 mm and a length of 30 mm. In the notched samples, an initial notch of 8 mm (40% of the total width) was made along the width direction from the sample edge toward the center of the sample using a sharp blade. The notched and unnotched samples were mounted in a tensile tester, while maintaining an initial length of 10 mm (distance between clamps), and the tensile testing was performed at a deformation rate of 500%/min. The critical displacement point (L_c) at which the crack in the notched sample began to propagate was determined by analyzing its prerecorded video. The fracture energy (Γ) was calculated using the following equation:

$$\Gamma = \frac{U(L_c)}{wt}, \qquad (1),$$

where $U(L_c)$ is the work done (area beneath the force–displacement curve) to deform an unnotched sample up to the L_c of the notched sample, and w and t are the width and thickness, respectively, of the unnotched sample.

Self-welding and lap shear tests. Self-welded cellulose and PVA GGs were fabricated, and their bonding strengths were evaluated using a lap shear test. To prepare the self-welded cellulose GG, two rectangular sheets of cellulose GG (thickness: ~2 mm) were first equilibrated in DMAc for ~1 d. The intended bonded parts of the gels were soaked in a cellulose/LiCl/DMAc solution (which was originally used as the precursor for cellulose gel fabrication) for 5 min, and subsequently joined with a longitudinal overlap of ~5 mm by gentle pressing, and thereafter exposed to ambient conditions for ~1 d for interfacial curing. Subsequently, the welded gel was soaked sequentially in ethanol and water for ~12 h each. Finally, the water in the welded gel was replaced by glycerol through a sequential solvent exchange process (0%→25%→50%→100% glycerol) to obtain the self-welded cellulose GG. To fabricate the self-welded PVA GG, the intended bonding parts of two rectangular sheets of PVA GG (fabricated from a 5 wt.% PVA precursor solution) of ~1.8 mm thickness were soaked in a $LiClO_4$/glycerol solution (20:80, w/w) at 140 °C for 15 min. Thereafter, the sheets were joined with a longitudinal overlap of ~5 mm by gentle pressing and exposed sequentially at 80 °C for 1 h and ambient temperature for ~12 h for interfacial curing. Finally, the welded PVA GG was equilibrated in pure glycerol to remove any free salt ions from the gel. To evaluate the bonding strength of the self-welded cellulose and PVA GGs via the lap shear test, a tensile test was performed at 500% of the initial length (distance between clamps) per min (500%/min) with the initial length being ~10 mm. The adhesive strength of the gel was determined by dividing the maximum force required for interfacial failure by the shear area (overlap length × width: 5 mm × 5 mm).

Fabrication of patterned glycerogels. A predesigned fractal-shaped silver pattern was created on a PVA GG surface using a mask-induced ion-sputtering method. A soft PVA GG sheet (40 mm × 30 mm × 1.7 mm) fabricated from a 4 wt.% precursor solution was used. A commercial ion-sputtering machine (Magnetron sputtering system, ALPHAPLUS, Republic of Korea) was used for the sputtering. The sample was covered with a predesigned mask and set on the sample holder, which was subsequently placed on the anode. Silver sputtering was carried out in vacuum (10^{-6} Torr pressure) with argon flow (flow rate 20 cm^3 min^{-1}) for 4 min under the application of a direct current of 2 A. Thereafter, the sample was extracted from the chamber, and the mask was removed to obtain the desired silver-patterned GG.

Fabrication of glycerogel-based electrolyte and supercapacitor. The PVA-GG-based electrolyte was fabricated using $LiClO_4$ as the salt ion source. Initially, a soft PVA gel was fabricated from a 5 wt.% precursor solution in DMSO/water (75:25, w/w) using a plastic mold of thickness 0.5 mm. Following freezing (-50 °C, 1 d) and thawing (25 °C, 12 h), the gel was sequentially equilibrated in 25% (12 h) and 50% (12 h) glycerol (w/w). Subsequently, the gel was equilibrated in a solution containing 20% $LiClO_4$ in 75% aqueous glycerol (w/w) for 1 d. Finally, the gel was equilibrated in a solution of 20% $LiClO_4$ in pure glycerol (w/w) for 1 d to obtain the as-prepared PVA GG electrolyte (thickness: ~0.2 mm). The gel electrolyte sheet was cut into squares of dimensions 20 mm × 20 mm and sandwiched between two parallel CNT films (20 mm × 20 mm), which served as the anode and cathode. The sandwiched CNT electrodes and PVA GG-$LiClO_4$ electrolyte were annealed in a closed glass vial at 90 °C for 3 h and slowly cooled to 25 °C to obtain the desired PVA GG electrolyte-based flexible supercapacitor (CNT/PVA GG-$LiClO_4$).

Electrochemical measurements. All electrochemical measurements of the fabricated PVA GG electrolyte and supercapacitor were conducted using a Metrohm Multi Autolab/M204 multichannel potentio-galvanostat (The Netherlands). The CNT/PVA GG-$LiClO_4$ supercapacitor (length × width × thickness: 20 mm × 20 mm × 0.2 mm) was sandwiched between two parallel copper plates, which were connected via wires to the potentio-galvanostat (Fig. 6a). Electrochemical impedance spectroscopy (EIS), cyclic voltammetry (CV), and GCD tests of the samples were carried out in two-electrode configurations. The sample-electrode setup was pre-equilibrated at the respective measurement temperatures for 30 min, whereafter the electrochemical measurements were performed by keeping the setup at the respective temperatures.

EIS was performed in the frequency range of 10^6–0.1 Hz at an amplitude of 10 mV. The highest-frequency value in the Nyquist plot was considered to be the bulk resistance (R) of the sample. The ionic conductivity (s) was calculated using the following equation:

$$\sigma = \frac{l}{RA}, \qquad (2),$$

where l is the thickness of the gel electrolyte and A is the cross-sectional surface area of the electrodes.

CV was performed from 0 to 1 V at scan rates of 1–50 mV s^{-1}. The areal capacitance of the supercapacitor C (mF cm^{-2}) from the CV curve was calculated using the following equation:

$$C = \frac{\int I(\mathrm{V})\mathrm{dV}}{2\nu A \Delta V}, \qquad (3),$$

where $\int I(\mathrm{V})\mathrm{dV}$ is the area inside the CV loop, n is the scan rate, A is the surface area of one electrode, and DV is the potential range.

GCD was performed from 0 to 1 V with the application of a current varying from 0.1 mA to 2 mA. The areal capacitance of supercapacitor C (mF cm^{-2}) was calculated from the GCD curve using the following equation:

$$C = \frac{I\Delta t}{2A\Delta V}, \qquad (4),$$

where I is the applied current, Dt is the discharge time, A is the surface area of the electrode, and DV is the potential range.

Declarations

Data availability

The data supporting the findings of this study are available within this article and its Supplementary Information files.

Acknowledgements

This study was supported by the National Research Foundation of Korea (NRF) grants funded by the Korea government (MSIT) (Nos. 2020R1A2C2007974 and 2021R1A4A1029780). Md.T.I.M. acknowledges the financial support from the Brain Pool program through the NRF funded by the MSIT (No. 2019H1D3A1A02070510).

Author contributions

Md.T.I.M. and I.J. conceived and designed the study. Md.T.I.M., Y.L., A.V.R.V., T.G., and R.R.M.W. performed experiments. All the authors discussed the results and contributed to data interpretation. Md.T.I.M. and I.J. wrote the manuscript.

Competing interests

The authors declare no competing interests.

References

1. Mredha, Md. T. I. & Jeon, I. Biomimetic anisotropic hydrogels: Advanced fabrication strategies, extraordinary functionalities, and broad applications. *Prog. Mater. Sci.* **124** (2022). 10.1016/j.pmatsci.2021.100870.

2. Mredha, Md. T. I. et al. Anisotropic tough double network hydrogel from fish collagen and its spontaneous in vivo bonding to bone. *Biomaterials* **132**, 85–95 (2017). 10.1016/j.biomaterials.2017.04.005.

3. Cianchetti, M., Laschi, C., Menciassi, A. & Dario, P. Biomedical applications of soft robotics. *Nat. Rev. Mater.* **3**, 143–153 (2018). 10.1038/s41578-018-0022-y.

4. Yuk, H., Lu, B. & Zhao, X. Hydrogel bioelectronics. *Chem. Soc. Rev.* **48**, 1642–1667 (2019). 10.1039/c8cs00595h.

5. Yang, C. & Suo, Z. Hydrogel ionotronics. *Nat. Rev. Mater.* **3**, 125–142 (2018). 10.1038/s41578-018-0018-7.

6. Style, R. W., Tutika, R., Kim, J. Y. & Bartlett, M. D. Solid-liquid composites for soft multifunctional materials. *Adv. Funct. Mater.* **31** (2021). 10.1002/adfm.202005804, 2005804.

7. Zhang, Y. S. & Khademhosseini, A. Advances in engineering hydrogels. *Science* **356**, 500 (2017). 10.1126/science.aaf3627.

8. Hao, X. P. et al. Kirigami-design-enabled hydrogel multimorphs with application as a multistate switch. *Adv. Mater.* **32**, e2000781 (2020). 10.1002/adma.202000781.

9. Jeon, I., Cui, J., Illeperuma, W. R. K., Aizenberg, J. & Vlassak, J. J. Extremely stretchable and fast self-healing hydrogels. *Adv. Mater.* **28**, 4678–4683 (2016). 10.1002/adma.201600480.

10. Tran, V. T. et al. Electrically, thermally, and mechanically anisotropic gels with a wide operational temperature range. *Adv. Funct. Mater.* (2021). 10.1002/adfm.202110177.

11. Mredha, Md. T. I. et al. A facile method to fabricate anisotropic hydrogels with perfectly aligned hierarchical fibrous structures. *Adv. Mater.* **30** (2018). 10.1002/adma.201704937, 29341264.

12. Mredha, Md. T. I. et al. Anisotropic tough multilayer hydrogels with programmable orientation. *Mater. Horiz.* **6**, 1504–1511 (2019). 10.1039/C9MH00320G.

13. Gong, J. P., Katsuyama, Y., Kurokawa, T. & Osada, Y. Double-network hydrogels with extremely high mechanical strength. *Adv. Mater.* **15**, 1155–1158 (2003). 10.1002/adma.200304907.

14. Sun, J. Y. et al. Highly stretchable and tough hydrogels. *Nature* **489**, 133-136 (2012). 10.1038/nature11409.

15. Haraguchi, K. & Takehisa, T. Nanocomposite hydrogels: A unique organic–inorganic network structure with extraordinary mechanical, optical, and swelling/de-swelling properties. *Adv. Mater.* **14**, 1120–1124 (2002). 10.1002/1521-4095(20020816)14:16<1120::AID-ADMA1120>3.0.CO;2-9.

16. Sun, T. L. et al. Physical hydrogels composed of polyampholytes demonstrate high toughness and viscoelasticity. *Nat. Mater.* **12**, 932–937 (2013). 10.1038/nmat3713.

17. Tran, V. T. et al. Conductive tough hydrogels with a staggered ion-coordinating structure for high self-recovery rate. *ACS Appl. Mater. Interfaces* **11**, 24598–24608 (2019). 10.1021/acsami.9b06478.

18. Mredha, Md. T. I., Pathak, S. K., Tran, V. T., Cui, J. & Jeon, I. Hydrogels with superior mechanical properties from the synergistic effect in hydrophobic–hydrophilic copolymers. *Chem. Eng. J.* **362**, 325–338 (2019). 10.1016/j.cej.2018.12.023.

19. Mredha, Md. T. I., Le, H. H., Cui, J. & Jeon, I. Double-hydrophobic-coating through quenching for hydrogels with strong resistance to both drying and swelling. *Adv. Sci. (Weinh)* **7**, 1903145 (2020). 10.1002/advs.201903145.

20. Jian, Y. et al. Biomimetic anti-freezing polymeric hydrogels: Keeping soft-wet materials active in cold environments. *Mater. Horiz.* **8**, 351–369 (2021). 10.1039/d0mh01029d.

21. Liu, J. et al. Metallopolymer organohydrogels with photo-controlled coordination crosslinks work properly below 0 °C. *Adv. Mater.* **32**, e1908324 (2020). 10.1002/adma.201908324.

22. Rong, Q., Lei, W., Huang, J. & Liu, M. Low temperature tolerant organohydrogel electrolytes for flexible solid-state supercapacitors. *Adv. Energy Mater.* **8** (2018). 10.1002/aenm.201801967.

23. Rong, Q. et al. Anti-freezing, conductive self-healing organohydrogels with stable strain-sensitivity at subzero temperatures. *Angew. Chem. Int Ed Engl* **56**, 14159–14163 (2017). 10.1002/anie.201708614.

24. Chen, F. et al. Rational fabrication of anti-freezing, non-drying tough organohydrogels by one-pot solvent displacement. *Angew. Chem. Int Ed Engl* **57**, 6568–6571 (2018). 10.1002/anie.201803366.

25. Horikawa, D. D. Survival of tardigrades in extreme environments: A model animal for astrobiology. *Cell. Orig. Life Extreme Habitats Astrobiol.* **21**, 205–217 (2012). 10.1007/978-94-007-1896-8_12.

26. Tsujimoto, M., Imura, S. & Kanda, H. Recovery and reproduction of an Antarctic tardigrade retrieved from a moss sample frozen for over 30 years. *Cryobiology* **72**, 78–81 (2016). 10.1016/j.cryobiol.2015.12.003.

27. Crowe, J. H. & Crowe, L. M. Preservation of mammalian cells–learning nature's tricks. *Nat. Biotechnol.* **18**, 145–146 (2000). 10.1038/72580.

28. Bertolani, R. et al. Experiences with dormancy in tardigrades. *J. Limnol.* **63**, 16–25 (2004). 10.4081/jlimnol.2004.s1.16.

29. Somme, L. Anhydrobiosis and cold tolerance in tardigrades. *Eur. J. Entomol.* **93**, 349-357 (1996).

30. Basiak, E., Lenart, A. & Debeaufort, F. How glycerol and water contents affect the structural and functional properties of starch-based edible films. *Polymers* **10**, 412 (2018). 10.3390/polym10040412.

31. Gu, Y. & Jérôme, F. Glycerol as a sustainable solvent for green chemistry. *Green Chem.* **12**, 1127–1138 (2010). 10.1039/c001628d.

32. Zondervan, R., Kulzer, F., Berkhout, G. C. G. & Orrit, M. Local viscosity of supercooled glycerol near T_g probed by rotational diffusion of ensembles and single dye molecules. *Proc. Natl Acad. Sci. U. S. A.* **104**, 12628–12633 (2007). 10.1073/pnas.0610521104, Pubmed:17488815.

33. Sato, K. et al. Phase-separation-induced anomalous stiffening, toughening, and self-healing of polyacrylamide gels. *Adv. Mater.* **27**, 6990–6998 (2015). 10.1002/adma.201502967.

34. Kim, J., Zhang, G., Shi, M. & Suo, Z. Fracture, fatigue, and friction of polymers in which entanglements greatly outnumber cross-links. *Science* **374**, 212–216 (2021). 10.1126/science.abg6320.

35. Roy, C. K. et al. Self-adjustable adhesion of polyampholyte hydrogels. *Adv. Mater.* **27**, 7344–7348 (2015). 10.1002/adma.201504059.

36. Elder, S., Clune, J., Walker, J. & Gloth, P. Suitability of EGCG as a means of stabilizing a porcine osteochondral xenograft. *J. Funct. Biomater.* **8**, 43 (2017). 10.3390/jfb8040043.

37. Nonoyama, T. et al. Double-network hydrogels strongly bondable to bones by spontaneous osteogenesis penetration. *Adv. Mater.* **28**, 6740–6745 (2016). 10.1002/adma.201601030.

38. Hu, Z., Chen, Y., Wang, C., Zheng, Y. & Li, Y. Polymer gels with engineered environmentally responsive surface patterns. *Nature* **393**, 149–152 (1998). 10.1038/30205.

39. Fan, J. A. et al. Fractal design concepts for stretchable electronics. *Nat. Commun.* **5**, 3266 (2014). 10.1038/ncomms4266.

40. Younesi, R., Veith, G. M., Johansson, P., Edström, K. & Vegge, T. Lithium salts for advanced lithium batteries: Li–metal, Li–O 2, and Li–S. *Energy Environ. Sci.* **8**, 1905-1922 (2015). 10.1039/C5EE01215E.

41. Vijayakumar, V. et al. An all-solid-state-supercapacitor possessing a non-aqueous gel polymer electrolyte prepared using a UV-assisted in situ polymerization strategy. *J. Mater. Chem. A* **5**, 8461–8476 (2017). 10.1039/C7TA01514C.

42. Lu, N. et al. Rational design of antifreezing organohydrogel electrolytes for flexible supercapacitors. *ACS Appl. Energy Mater.* **3**, 1944–1951 (2020). 10.1021/acsaem.9b02379.

43. Lu, C. & Chen, X. All-temperature flexible supercapacitors enabled by antifreezing and thermally stable hydrogel electrolyte. *Nano Lett.* **20**, 1907–1914 (2020). 10.1021/acs.nanolett.9b05148.

44. Li, X. et al. Flexible supercapacitor based on organohydrogel electrolyte with long-term anti-freezing and anti-drying property. *Adv. Funct. Mater.* **30**, 2007291 (2020). 10.1002/adfm.202007291.

45. Feng, J. et al. Metallic few-layered VS_2 ultrathin nanosheets: High two-dimensional conductivity for in-plane supercapacitors. *J. Am. Chem. Soc.* **133**, 17832–17838 (2011). 10.1021/ja207176c.

46. El-Kady, M. F., Strong, V., Dubin, S. & Kaner, R. B. Laser scribing of high-performance and flexible graphene-based electrochemical capacitors. *Science* **335**, 1326–1330 (2012). 10.1126/science.1216744.

47. Qin, J. et al. 2D mesoporous MnO_2 nanosheets for high-energy asymmetric micro-supercapacitors in water-in-salt gel electrolyte. *Energy Storage Mater.* **18**, 397–404 (2019). 10.1016/j.ensm.2018.12.022.

48. Guo, H. et al. All-in-one shape-adaptive self-charging power package for wearable electronics. *ACS Nano* **10**, 10580–10588 (2016). 10.1021/acsnano.6b06621.

49. Guo, Y., Zheng, K. & Wan, P. A flexible stretchable hydrogel electrolyte for healable all-in-one configured supercapacitors. *Small* **14**, e1704497 (2018). 10.1002/smll.201704497.

50. Trieu, H. & Qutubuddin, S. Poly(vinyl alcohol) hydrogels: 2. Effects of processing parameters on structure and properties. *Polymer* **36**, 2531–2539 (1995). 10.1016/0032-3861(95)91198-G.

Figures

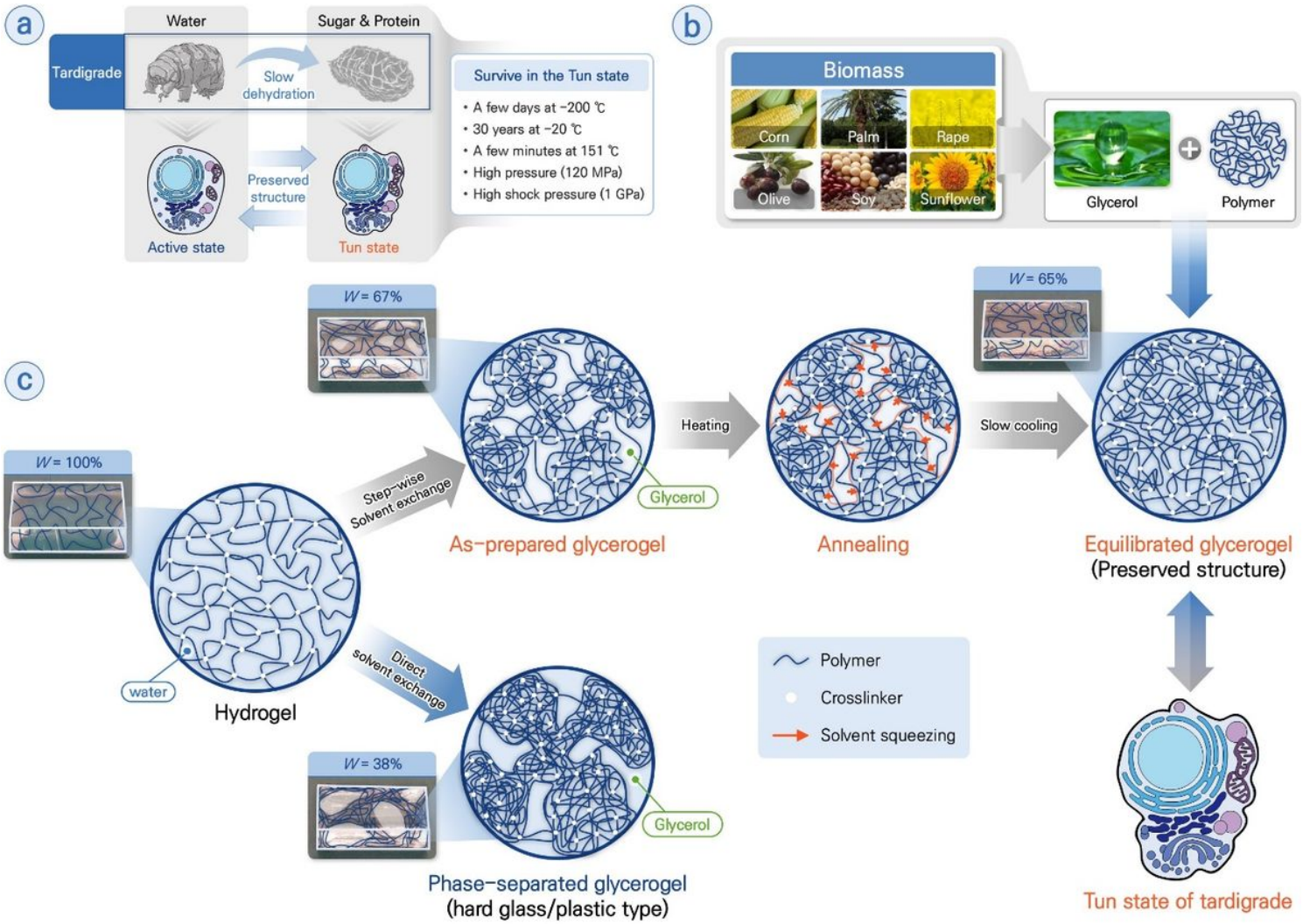

Figure 1

Bioinspired strategy for designing extremotolerant GGs. a. Tardigrades can transform into a “tun state” under extreme conditions by preserving their integral structure, which can survive various harsh environmental challenges. **b**. Inspired by the tun formation of tardigrades, extremotolerant multifunctional GGs were designed by integrating various polymers with a green solvent (glycerol). **c**. Initially, the water contained in the predesigned functional hydrogels was replaced with glycerol sequentially to minimize damage to the integral structure of the gel. Thereafter, the as-prepared GG was dry-annealed to release undesired residual stresses and obtain the final GG having a preserved polymer structure similar to the tun formation of tardigrades. In contrast, direct solvent exchange resulted in a phase-separated hard structure inside the gel network.

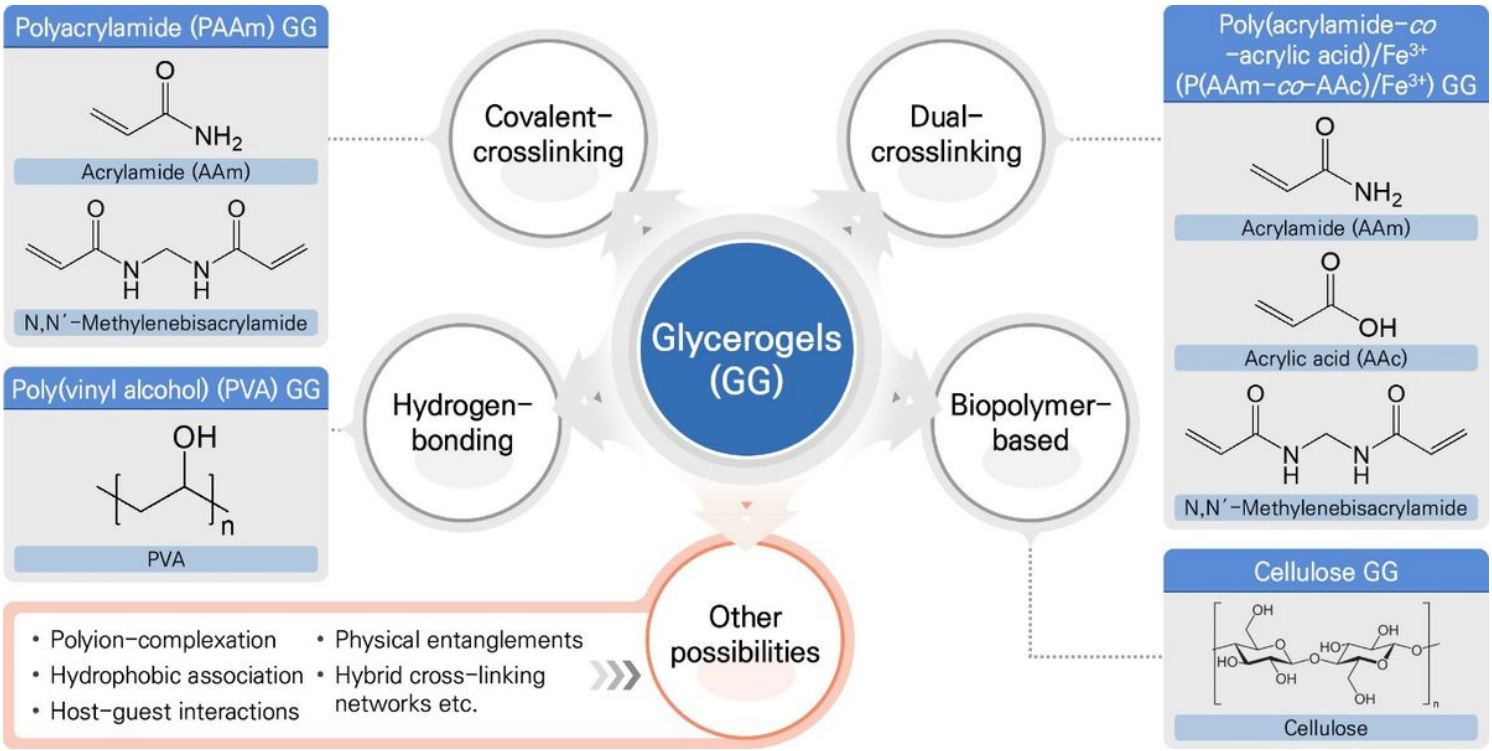

Figure 2

Different monomers/polymers and crosslinkers used for designing GGs. The versatility of the method facilitates the design of a wide range of multifunctional GGs.

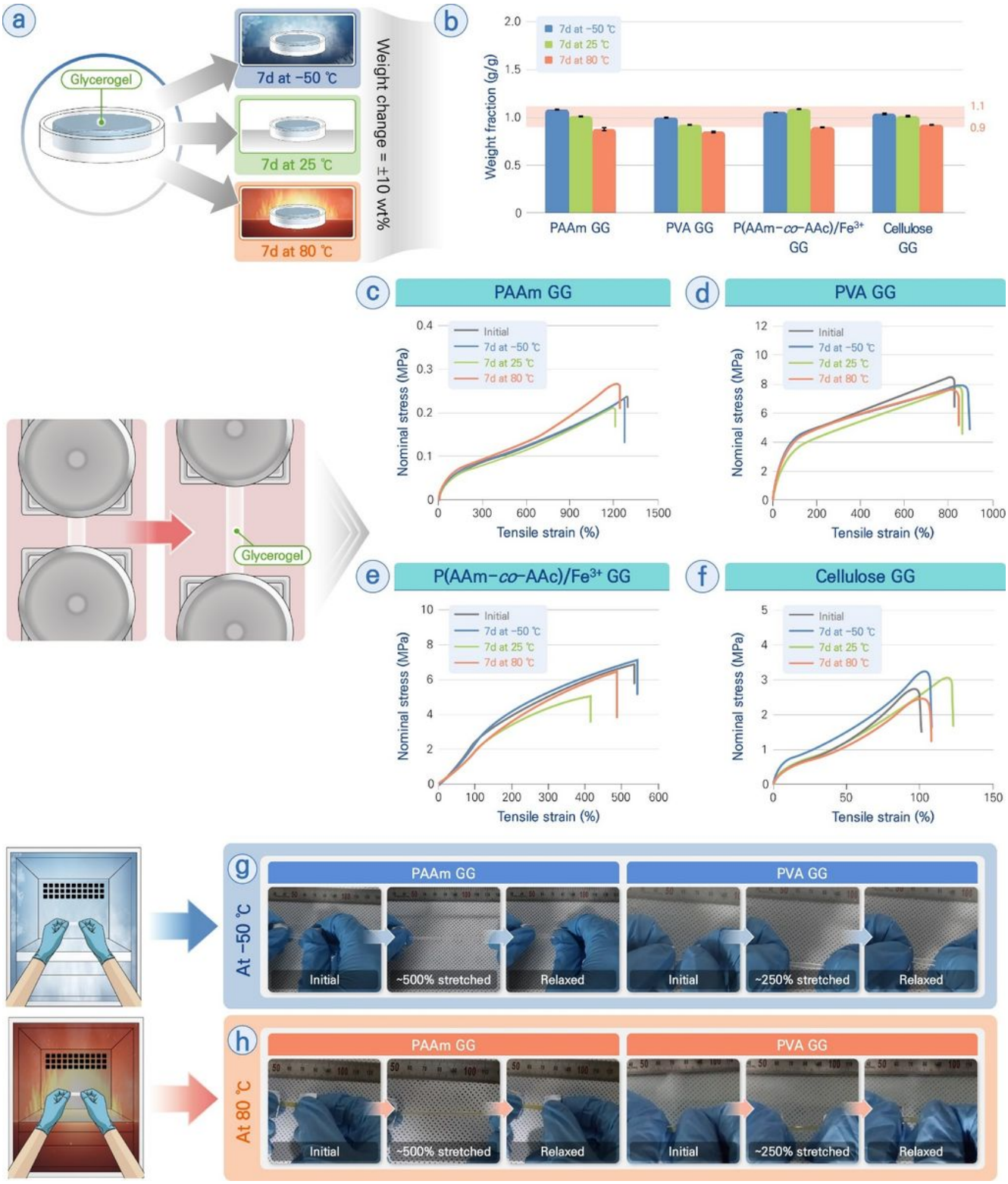

Figure 3

Characterization of the extremotolerant ability of GGs. a. Observation of the effect of low (-50 °C), ambient (25 °C), and high (80 °C) temperatures on the as-developed GGs. **b**. Weight fractions of the GGs following incubation for 7 d incubation at -50, 25 °C, and 80 °C. Representative tensile stress-strain curves of **c**. PAAm, **d**. PVA, **e**. P(AAm-*co*-AAc)/Fe^{3+}, and **f**. cellulose GGs. Tensile tests were performed on pristine samples, and results were compared with those of the samples were incubated at -50, 25, and 80 °C for 7

d. Demonstration of the stretchability of PAAm and PVA GGs following incubation them for 7 d at **g**. -50 °C and **h**. 80 °C.

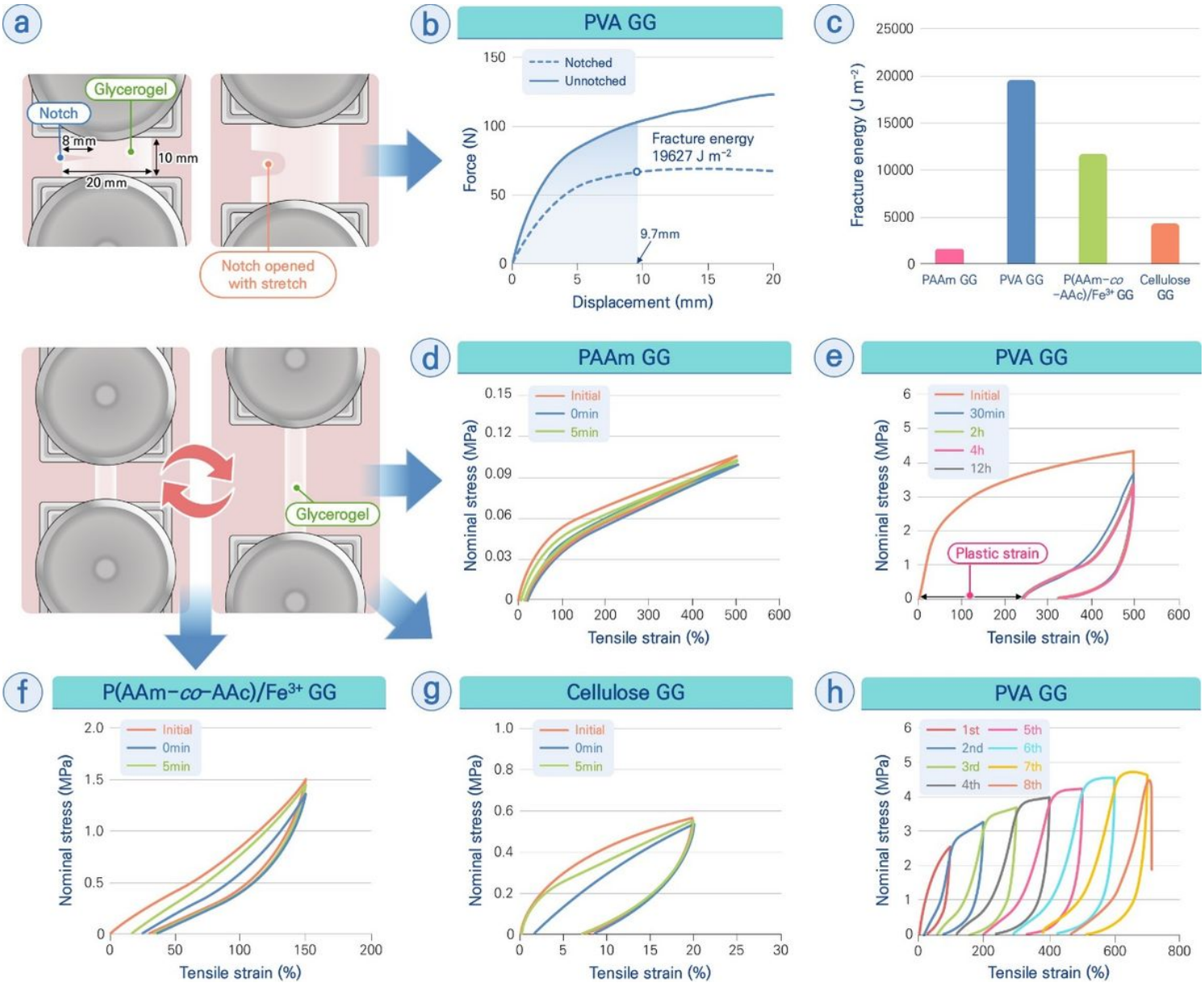

Figure 4

Fracture toughness, hysteresis, elasticity, and plasticity of GGs. a. Demonstration of the tensile test of a notched sample for the determination of fracture energy. **b**. Force vs. displacement curves of a notched and an unnotched sample of PVA GG. The critical displacement (L_c) at which the crack began propagating through the notched sample (detected by video analyses) was identified by an open circle. Fracture energy was determined by dividing the work done (filled area) to stretch the unnotched sample up to the L_c by the cross-sectional area of the sample. **c**. Determined fracture energies of different GGs. Repeated tensile loading–unloading curves of **d**. PAAm GG, **e**. PVA GG, **f**. P(AAm-co-AAc)/Fe^{3+} GG, and **g**. cellulose GG at different waiting times. **h**. Repeated tensile loading–unloading curves of PVA GG with a periodical enhancement in strain by 100% up to its fracture point.

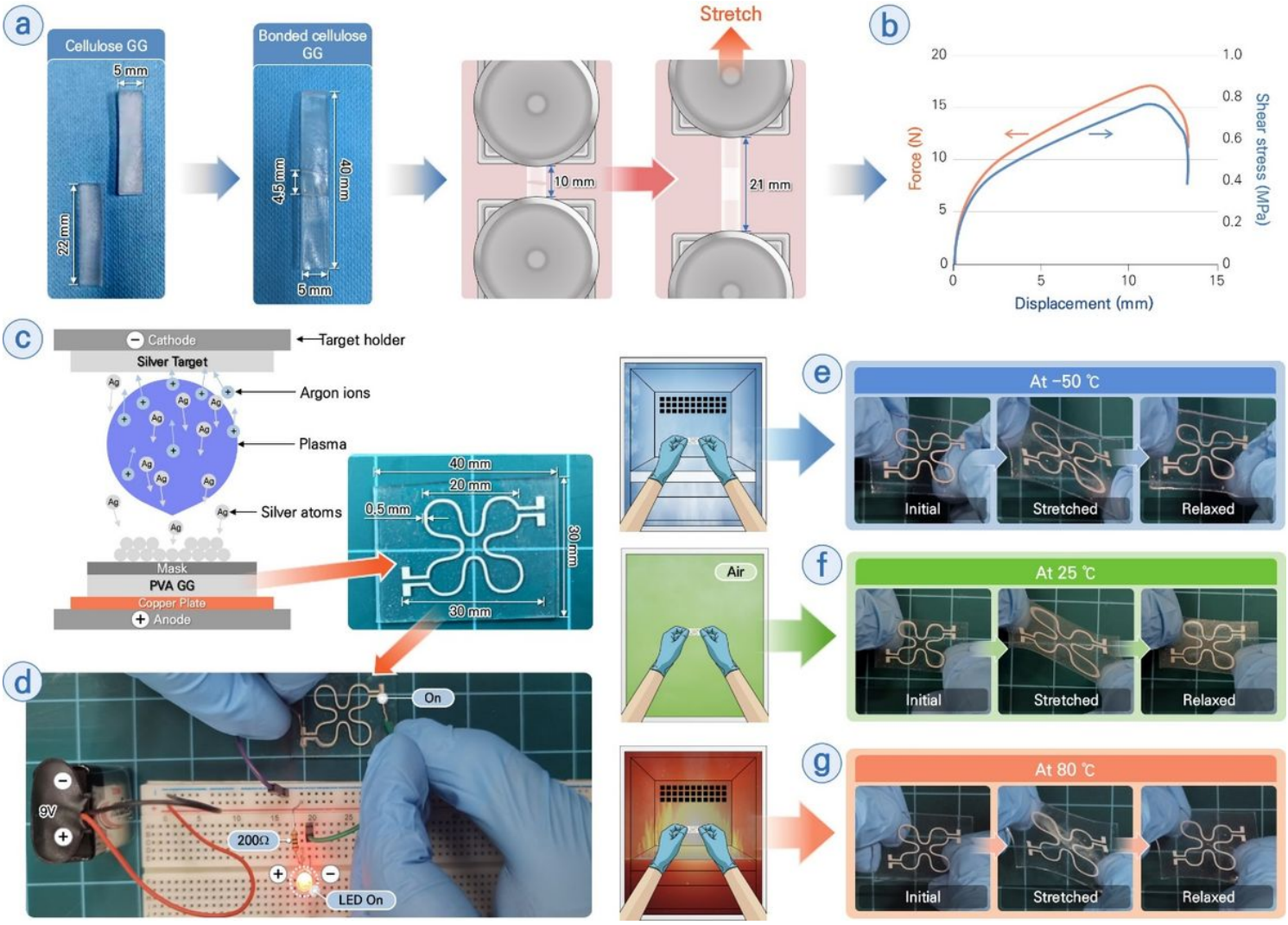

Figure 5

GG-based self-welding and stretchable electrical pattern. **a**. Demonstration of self-welding process of cellulose GG. **b**. Lap shear test to determine the shear adhesive force and strength of welded cellulose GG. **c**. Illustration and photograph of a silver-patterned PVA GG fabricated by a mask-controlled ion-sputtering process. **d**. LED switching by patterned PVA GG connected to a 9 V battery through with a 200 W resistor. **e–g**. Demonstration of the stretchability of the patterned PVA GG at -50, 25, and 80 °C.

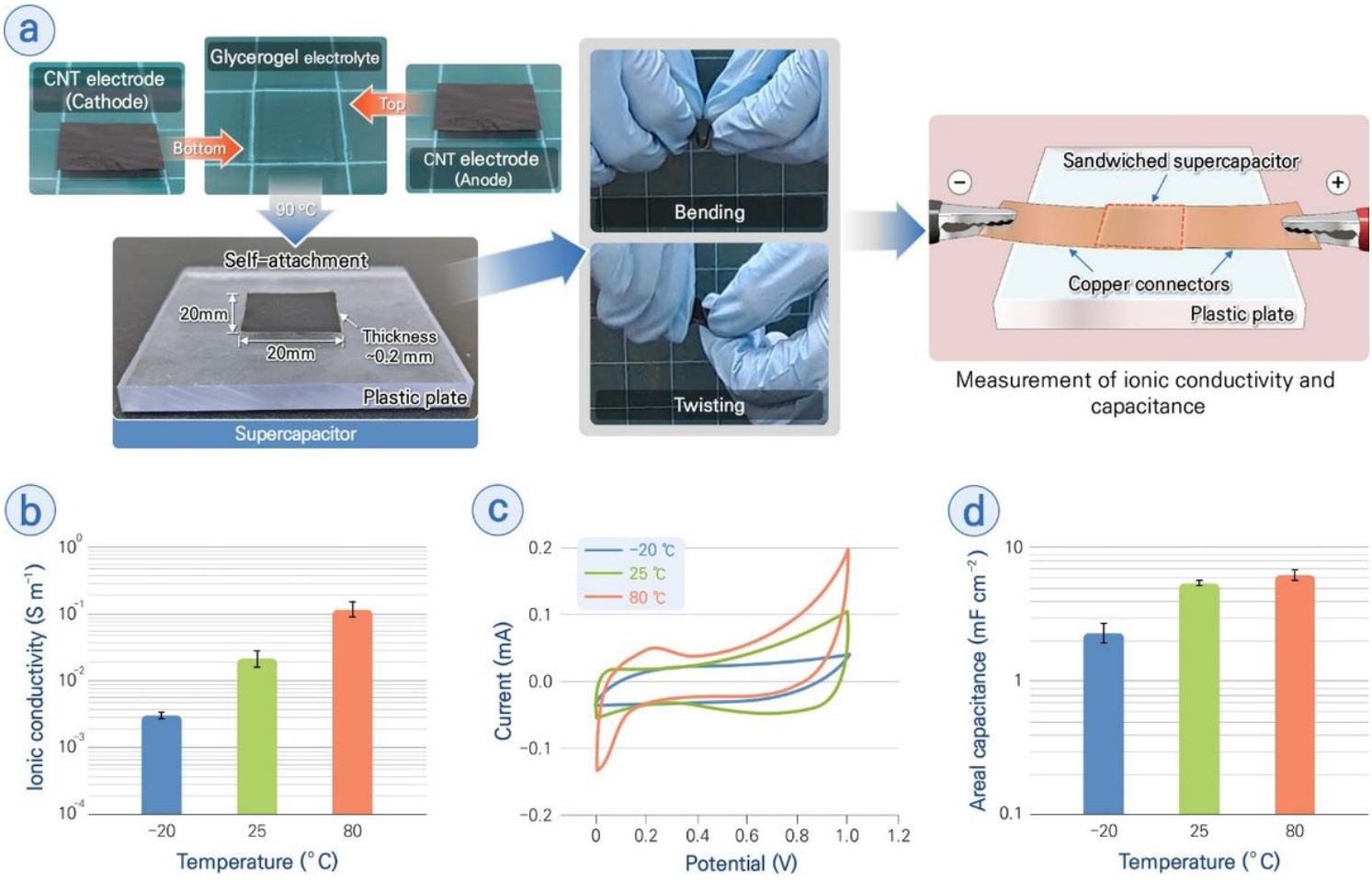

Figure 6

GG-based flexible electrolyte and supercapacitor. a. Fabrication and characterizations of flexible PVA GG electrolyte-based supercapacitor. **b**. Ionic conductivities of PVA GG electrolyte at different temperatures. **c.** CV profiles recorded at the scan rate of 1 mV s^{-1}, and **d.** calculated areal capacitance of the supercapacitor device measured at different temperatures.

Supplementary Files

This is a list of supplementary files associated with this preprint. Click to download.

- SupplementaryMovieS1.mp4
- SupplementaryMovieS2.mp4
- SupplementaryMovieS3.mp4
- SupplementaryMovieS4.mp4
- SupplementaryMovieS5.mp4
- SupplementaryMovieS6.mp4
- SupplementaryMovieS7.mp4

- SupplementaryMovieS8.mp4
- SupplementaryMovieS9.mp4
- 02SupplementaryInformationGlycerogelsTarifulJeonMar212022.docx